Delayed feedback dynamics of Lienard-type resonant tunneling-photo-detector optoelectronic oscillators

Delayed Feedback Dynamics of Liénard-Type Resonant Tunneling-Photo-Detector Optoelectronic Oscillators

Bruno Romeira, *Student Member, IEEE*, Julien Javaloyes, *Member, IEEE*, José M. L. Figueiredo, *Member, IEEE*, Charles N. Ironside, *Senior Member, IEEE*, Horacio I. Cantú, and Anthony E. Kelly

***Abstract*— We use the nonlinear dynamics approach for studying delayed feedback optoelectronic oscillators (OEOs) formed by hybrid integration of resonant tunneling diode (RTD) photodetectors with laser diodes, in both single and dual optical fiber feedback routes. In the single loop topology, the performance of the RTD-OEO free-running self-sustained oscillator is improved in terms of phase noise, with a compromise between the delay line and the strength of the optical re-injection. In the dual-loop configuration, superior performance is achieved due to the suppression of the side modes associated with the optical cavity length, resulting in a side mode suppression ratio of up to −60 dBc of the carrier frequency. We compare experimental results with numerical simulations based on a system of delay differential equations comprising a Liénard oscillator model driven by white Gaussian noise and coupled with laser rate equations. The delayed feedback Liénard oscillator model gives considerable insight into the RTD-OEO dynamical regimes predicting its main features in both single- and dual-loop configurations.**

***Index Terms*— Delay differential equations, delay lines, laser diode, optoelectronic oscillator (OEO), photo-detector, resonant tunneling diodes.**

I. Introduction

DELAYED feedback systems are common in scientific fields such as physiology, biology, chemistry, and laser systems [1]. Depending on how it is configured adding a delayed feedback loop to a system can stabilize the output producing highly stable periodic waveforms [2], or it can produce exceedingly complex dynamics, namely chaos [3]–[5]. Furthermore, it has been demonstrated that the dynamics of such systems can be easily synchronized and controlled using either external perturbation or feedback parameters [6], [7].

The effect of the delayed feedback is to reinject into the system one or more state variables, with a delay. Within the field of laser dynamics, the most prominent examples are the optoelectronic feedback [8], the optical feedback [9]–[11], and the optoelectronic oscillator (OEO) [2] configurations. The optoelectronic feedback consists of current re-injection of the detected laser output using a fast responding photodiode, which produces a current that is an image of the laser output power and that is added, after a delay time, to the laser driving current. In external optical feedback of laser systems, an external mirror is used to optically re-inject a fraction of the light produced by the laser into its active region, and the round-trip time of light in the external cavity introduces a delay. In OEO systems, external elements (electro-optic modulators, RF oscillators, etc.) are used to produce nonlinearities, and the laser diode (LD) is used only as a light source.

Optoelectronic oscillators combining electronic and photonic components have been intensively studied to achieve stable and high purity RF signals. A typical OEO includes a laser source, an intensity modulator, a photodetector, a band-pass filter, and an RF amplifier in an optical fiber single loop configuration [2]. Nowadays, the number of reported single-loop OEO architectures is considerably large and spans from OEOs based on several modulator types to implementations using whispering gallery mode (WGM) cavities, and OEOs with fiber lasers, among others (for a review see [12]). Dual-loop OEO topologies have been also proposed to overcome the limitations of the appearance of very strong side mode peaks in fiber-based single loops [13]–[15].

Other OEO configurations have been reported utilizing self-injection locking of microwave oscillators for compact and low cost OEOs. As an example, high-purity OEO topologies were demonstrated utilizing indium phosphide heterojunction bipolar transistor (InP HBT) microwave oscillators monolithically integrated with photodiodes [16]. More recently, it was demonstrated for the first time a stable low-phase noise OEO comprising a resonant tunneling diode (RTD) monolithically integrated with a waveguide photo-detector (PD), and hybrid integrated with a laser diode, and an optical fiber delay line [17], as shown in the block diagram of Fig. 1.

Manuscript received September 17, 2012; accepted October 14, 2012. Date of publication October 18, 2012; date of current version November 29, 2012. This work was supported in part by the Fundação para a Ciência e Tecnologia Project under Grant WOWi-PTDC/EEA-EL/100755/2008. The work of B. Romeira was supported by FCT Ph.D. under Grant SFRH/BD/43433/2008. The work of J. Javaloyes was supported by the Ramón y Cajal Program as well as the Direcció General de Recerca, Desenvolupament Tecnològic i Innovació de la Conselleria d'Innovació, Interior i Justícia del Govern de les Illes Balears co-funded by the European Union FEDER funds.

B. Romeira, J. M. L. Figueiredo, and H. I. Cantú are with the Departamento de Física, Centro de Electrónica, Optoelectrónica e Telecomunicacções, Universidade do Algarve, Faro 8005-139, Portugal (e-mail: bmromeira@ualg.pt; jlongras@ualg.pt; hiquirino@ualg.pt).

J. Javaloyes is with the Departament de Fisica, Universitat de les Illes Baleares, Palma E-07122, Spain (e-mail: julien.javaloyes@uib.es).

C. N. Ironside and A. E. Kelly are with the School of Engineering, University of Glasgow, Glasgow G12 8LT, U.K. (e-mail: charles.ironside@glasgow.ac.uk; anthony.kelly@glasgow.ac.uk).

Color versions of one or more of the figures in this paper are available online at http://ieeexplore.ieee.org.

Digital Object Identifier 10.1109/JQE.2012.2225415

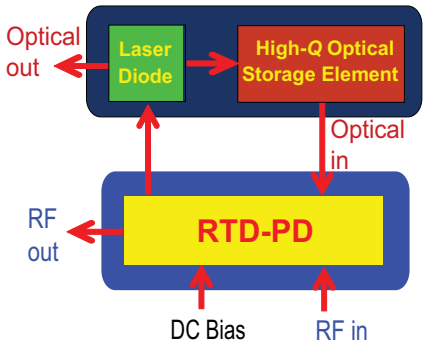

Fig. 1. Block diagram of the time delayed feedback RTD-OEO system.

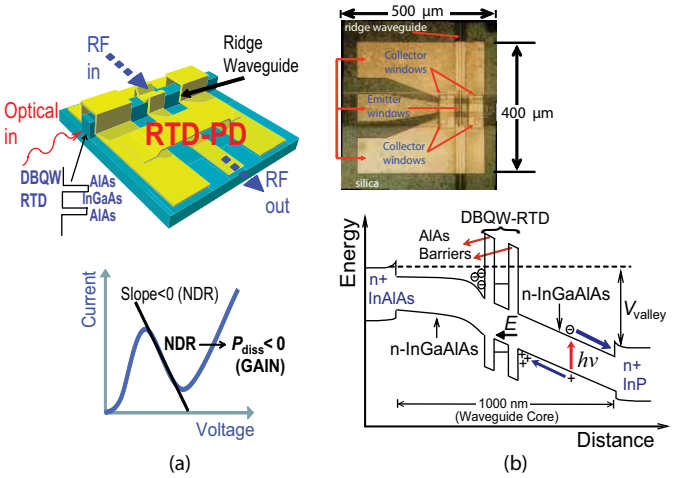

Fig. 2. (a) Schematic diagram of RTD-PD device showing the ridge optical waveguide and the DBQW region. RTD-PD's nonlinear current-voltage characteristic showing the NDR region. (b) RTD die top view showing the emitter and collector windows and the ridge waveguide (the ridge waveguide defines the device active area). RTD-PD unipolar InAlAs/$In_{0.53}Ga_{0.42}Al_{0.05}As$/InP band energy diagram.

The RTD-PD-based OEO has low power requirements (the circuits employed in the OEO reported here consumed typically less than 70 mW electrical power) without the need of extra high-speed high-cost components such as electrical amplifiers, photo-detectors or modulators. Moreover, the RTD-OEO differs from conventional OEO systems because when the optical fiber loop is open (high-Q storage element in Fig. 1), self-sustained relaxation oscillations are still present which can be used for electrical [18] or optical [19], [20] injection locking in microwave-photonics applications [21]. This means that instead of producing the microwave oscillation, as in typical OEO configurations, the feedback loop in the RTD-OEO leads to the injection locking with a delayed replica of self-sustained oscillations.

In this paper, we present a comprehensive study of single and dual-loop RTD-PD-based OEOs. We investigate how a nonlinear dynamics system based upon delay differential equations (DDEs) can be applied to help to understand resonant tunneling diode optoelectronic oscillators which can give rise to new technologies that are inherently nonlinear and of complex analysis. The numerical model comprises a delayed feedback Liénard oscillator system driven by white Gaussian noise and coupled to laser rate equations. Although based on a large number of fitting parameters the model discussed here captures well the main features of RTD-OEO dynamics, including the free-spectral range (FSR) and the side mode suppression ratio (SMSR) of single and dual loop configurations. Moreover, the model does not require excessive long-lasting computational simulations usually required in the analysis of DDE systems.

The delayed feedback Liénard OEO presented here provides a simple way to study time delayed feedback OEO dynamical systems containing negative resistance oscillators. Furthermore, the model can be extended to include RTD-OEO's different noise characteristics in order to better describe quantitatively our OEO providing an useful tool for design purposes as well as to investigate the complex behavior of RTD-based oscillators induced by the delayed feedback.

The outline of this paper is as follows. In section II we start with a description of the RTD-PD, and the time-delayed feedback RTD-OEO experimental setup and its operating principle. In section III the numerical model of the RTD-OEO based on a system of DDEs with white Gaussian noise input is presented. In section IV we show the experimental and numerical results of the single loop RTD-OEO configuration. Section V follows with the results of a dual loop RTD-OEO configuration and a comparison with state of the art OEOs. In section VI we present the conclusions of our work.

II. RTD-PD Description and OEO Setup

The RTD-PD is a double barrier quantum well (DBQW) device embedded with an optical waveguide structure [22], Fig. 2, that shows the typical nonlinear current-voltage (I-V) characteristic of RTD devices with a negative differential resistance (NDR) region, inset of Fig. 2(a). Such structure provides at the same time light detection, electrical gain, and very high-speed functionalities [23] (although in this work we only present results in the microwave low band of the spectrum). The RTD-PD functions as a waveguide photo-detector with energy close to or above the waveguide core bandgap energy. Its structure was grown by molecular beam epitaxy in a Varian Gen II system on a n^+ InP substrate and consisted of 2-nm-thick AlAs barriers separated by a 6-nm-wide InGaAs, embedded in a 1 μm thick ridge waveguide RTD-PD which correspond to the photoconductive layers, as shown in the energy-band diagram of Fig. 2(b). The ridge waveguide consisted of an RTD-PD unipolar InAlAs/$In_{0.53}Ga_{0.42}Al_{0.05}As$/InP structure (for more detail see [19], [22]).

The RTD-PD-LD consists of an RTD monolithic integrated within a waveguide photo-detector connected in series with a laser diode chip mounted on a high-speed carrier submount and wire bonded to a 50 Ω printed circuit board microstrip line, Fig. 3. The continuous wave (CW) laser diode operated around 1550 nm with 6 mA threshold current and 0.23 W/A efficiency. The transmission line was used to interconnect with the 1 μF shunt capacitor and also to provide an output port for the generated RF power. The RF power was measured and the DC bias was provided through a bias-T. (For a detailed description of RTD-based optoelectronic circuits see [24].) As depicted in Fig. 3(a) and shown schematically in Fig. 3(b),

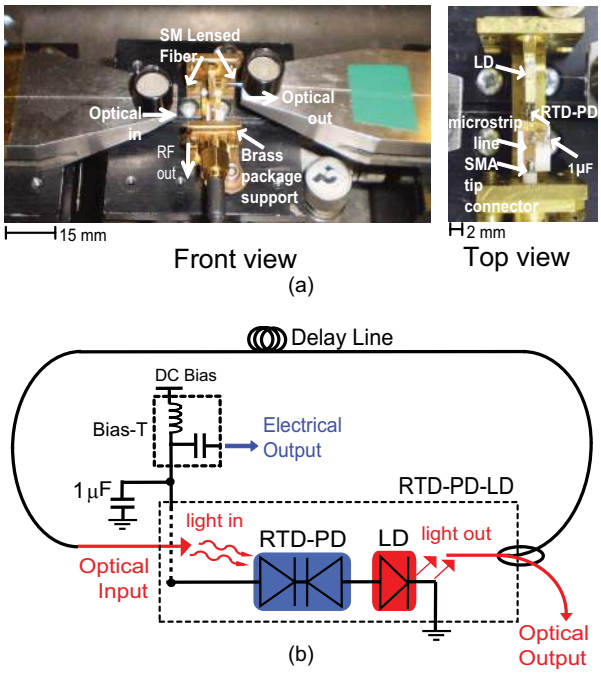

Fig. 3. (a) Front and top view pictures of the implemented RTD-PD-LD oscillator mounted on a three-axis stage with both optical input and output ports and an RF port. Also shown is the free-space light coupling and decoupling using lensed SMFs. (b) Schematic diagram of the single-loop RTD-OEO.

with this topology, we obtain a circuit with both optical input and output ports that allows to operate the RTD-PD-LD in several OEO modes.

When the RTD-PD in series with the LD are both connected in parallel with a 1 μF shunt capacitor, Fig. 3(b), and biased in NDR region of the RTD-PD-LD I-V curve, Fig. 4, the shunt capacitor works as a feedback element that helps sustain steady state oscillations whose frequency is imposed mainly by the LC circuit resonant tank $f_0 \simeq 1/2\pi\sqrt{LC}$, where L is the equivalent inductance from the gold wires and transmission line, and C stands for the RTD-PD's equivalent capacitance, Fig. 5. The RTD-PD relaxation self-sustained current oscillations drive the laser diode and the RTD-PD-LD works as an optoelectronic voltage controlled oscillator (OVCO) [18], [25] since its free-running frequency can be controlled by adjusting the DC bias voltage. Figure 4 presents the frequency tuning range when the DC voltage was scanned across the NDR region. The circuit used in the experiments oscillate with natural frequency ranging from 0.944 GHz to 1.129 GHz (that was mainly imposed by the wire bonding length of ~3-4 mm, and RTD-PD's active area of 150 μm $\times$ 4 μm).

For operation in the delayed-feedback mode, as represented schematically in Fig. 3(b), a fraction of the laser diode optical output was decoupled using a lensed single mode fiber (SMF), and sent through an optical fiber delay line to be launched into the RTD-PD using a similar lensed SMF, Fig. 3(a). Because a fraction of the laser modulated optical output (after passing through a long optical delay line) is launched into the RTD photo-detection region, the optical delay line provides a feedback route for self-injection locking which takes advantage of the optical fiber very low loss and large high-Q.

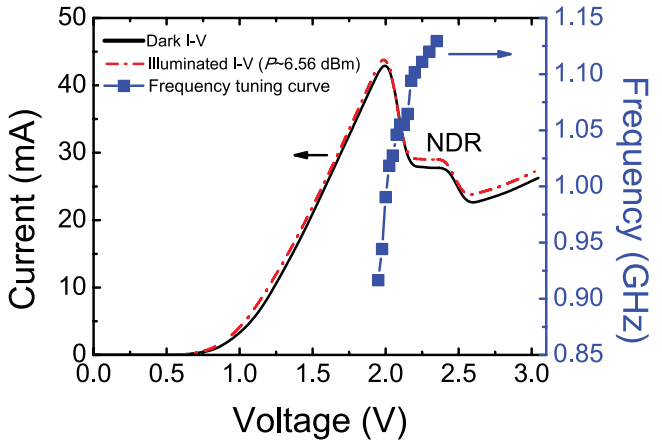

Fig. 4. Dark and illuminated $I-V$ characteristics of the RTD-PD device in series with the LD showing the NDR region. The corresponding frequency tuning curve in dark conditions as a function of the bias voltage is also plotted.

The experiments were performed without temperature or vibration control of the fiber loops. In this setup configuration, the RTD-OEO is a simple OEO with low power requirements (< 70 mW electrical power consumed by the RTD-PD-LD circuitry). The RTD-PD drives the laser diode with a microwave carrier, detects a fraction of the laser diode modulated optical output traveling in the optical fiber feedback loop, and provides wide bandwidth electronic gain which produces the self-sustained oscillations.

III. Description of the Model

Developing a computational model of the RTD-OEO capable of reproducing the diverse dynamical effects observed experimentally, namely the level of the side modes due to the long delay line and the various noise sources, can be a challenging task because of the different noise sources of the system. Moreover, since the round trip time scale corresponding to the optical fiber cavity mode spacing is much higher (typically in the μs range) than the time scale of the oscillation frequency of the oscillator, long run simulations and large amount of memory storage are usually required leading to time consuming simulations. In this section, we present a comprehensive numerical model of the single-loop delayed-feedback RTD-OEO system using delay differential equations. The model comprises a time-delayed feedback Liénard oscillator that models the RTD electrical dynamics with feedback control of the OEO, laser rate equations describing the LD dynamics, and a white Gaussian noise source which describes the dominant OEO noise sources, the thermal and shot noises.

A. RTD-PD Model

The dynamics of the RTD-PD oscillator is analyzed considering the lumped electrical circuit of Fig. 5. This circuit is equivalent to a Liénard oscillator [18], [25], that includes photocurrent (I_{ph}) and current noise (I_n) terms. The RTD-PD is represented by its intrinsic capacitance in parallel with a voltage dependent current source $F(V)$, and its photodetection behavior is modeled as an optical power modulated optical output dependent current source, I_{ph} [19]. The analysis presented

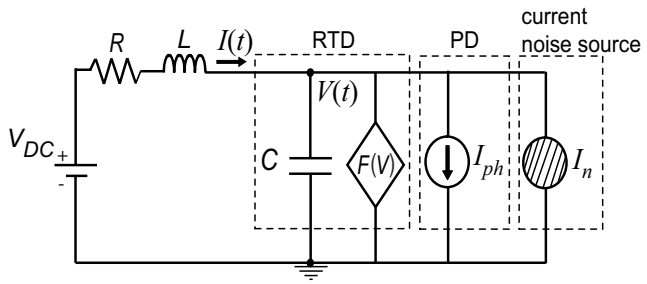

Fig. 5. Equivalent electrical circuit schematic of the resonant tunneling diode photo-detector oscillator with current noise injection. The resistor R and inductor L account for the circuit's series and parasitic resistance and inductance of RTD-PD-LD circuit, respectively.

here is valid for circuits where the RC time dominates over the depletion layer transit time and resonant state lifetime, i.e., the parasitic components of the hybrid circuit determines the frequency of oscillation.

By applying Kirchhoff's rules (using Faraday's law) to the circuit of Fig. 5, the voltage $V(t)$ across the capacitance C and the current $I(t)$ through the inductor L are given by the following set of two first-order autonomous differential equations, which correspond to the generalized Liénard system with current injection (photocurrent and Gaussian noise):

$$\dot{V}(t) = \frac{1}{C}\left[I(t) - F(V) - I_n - I_{ph}\right] \tag{1}$$

$$\dot{I}(t) = \frac{1}{L}\left[V_{DC} - RI(t) - V(t)\right] \tag{2}$$

where $F(V)$ is the mathematical representation of the RTD-PD current-voltage characteristic given by [26]. Although the DC I-V characteristic of the RTD-PD is a function of both voltage and optical power, in this work to avoid large running times simulations and reduce as much as possible the number of parameters, we assumed a static model of the I-V curve in the dark conditions. As shown in Fig. 4, under the moderate illuminated conditions employed in this work and considering the responsivity levels of the RTD-PDs used (below 0.25 A/W, Table I) the RTD-PD-LD I-V shifts slightly to lower voltages due to the generated photo-current without having a great effect on the overall I-V characteristic. In the cases where the optical re-injection changes substantially the I-V characteristic reducing their peak-to-valley ratio, and therefore the NDR region, refinements of the model can be employed using, for example, the ones reported in [27], that include the effect of light on the static DC current-voltage model taking into account the photoconductivity, and charge accumulation effects in double-barrier RTD structures.

In Eq. (1) the RTD-PD photo-generated current I_{ph} in response to a modulated optical signal $P(\lambda)$ is given by:

$$I_{ph} = \eta_{ph}\frac{e\lambda}{hc}P(\lambda) \tag{3}$$

where λ is the operation wavelength, e is the electric charge unit, h and c are the Planck constant and the speed of light in the vacuum, respectively, and η_{ph} is the waveguide photo-detector quantum efficiency given by:

$$\eta_{ph} = \kappa(1 - R_{ref})(1 - e^{-\alpha\gamma_{ph}\Lambda}), \tag{4}$$

with κ being the light coupling factor, R_{ref} is the waveguide facet reflectivity, α is the waveguide core absorption coefficient, γ_{ph} is the overlap integral of the electric and the optical fields, and Λ is the active waveguide PD length. Table I summarizes the typical values used in the simulations, estimated from the detection characteristics of experimental RTD-PD devices [19].

TABLE I
PARAMETERS OF THE ELECTRICAL CIRCUIT AND OF THE RTD WAVEGUIDE PHOTO-DETECTOR

Symbol	Quantity	Typical Order of Magnitude
R	Resistance	7.8 Ω
L	Inductance	3.1×10^{-9} H
C	Capacitance	3.25×10^{-12} F
λ	Operation wavelength	1.55 μm
κ	Light coupling factor	0.35
R_{ref}	Waveguide facet reflectivity	0.3
α_v	Waveguide core absorption coefficient (valley)	400 cm^{-1}
γ_{ph}	Overlap integral of the electric and optical fields	0.25
Λ	Waveguide contact length	150 μm

B. LD Model

In order to correlate the response of the laser diode to its physical parameters we use single-mode rate equations to describe its dynamic behavior. The rate equations for the photon $S(t)$ and injected carrier $N(t)$ densities in the active region are:

$$\dot{N}(t) = \frac{I_m(t)}{q\vartheta_{act}} - \frac{N(t)}{\tau_n} - g_0\{N(t) - N_0\} \times\{1 - \epsilon_n S(t)\}S(t) \tag{5}$$

$$\dot{S}(t) = \Gamma g_0\{N(t) - N_0\}\{1 - \epsilon_n S(t)\} \times S(t) - \frac{S(t)}{\tau_p} + \Gamma\beta\frac{N(t)}{\tau_n} \tag{6}$$

$$\frac{S(t)}{P_f} = \frac{\Gamma\tau_p\lambda_0}{V_{act}\eta_l hc} \tag{7}$$

where $I_m(t)$ is the oscillatory modulated current produced by the RTD-PD [given by Liénard's model, Eqs. (1) and (2)], plus the DC bias current I_{DC} to ensure the laser is on, ϑ_{act} is the laser active region volume, τ_n and τ_p are the spontaneous electron and photon lifetimes, respectively; the spontaneous emission factor β is the fraction of the spontaneous emission that is coupled to the lasing mode; N_0 is the carrier density for transparency, and g_0 is the is the differential gain; ϵ_n is the value for the nonlinear gain compression factor; Γ is the optical confinement factor; λ_0 is the emission wavelength; η_l

is the differential quantum efficiency per facet; and P_f is the laser output power.

C. Dimensionless Delayed Feedback Liénard OEO Model

In order to normalize Eqs. (1) and (2), we choose V_0 and I_0 as scale parameters with physical dimensions of current and voltage ($I_0 = 1$ A and $V_0 = 1$ V), respectively, and rescale $V(t) = x(t)V_0$, $I(t) = y(t)I_0$, $t = \tau(\omega_0)^{-1}$, $V_{DC} = v_0 V_0$, $\omega_0 = (\sqrt{LC})^{-1}$, and $R = \gamma\,(V_0/I_0)$. Variables $x(t)$ and $y(t)$ are dimensionless. The dimensionless single mode rate equations are obtained making use of the normalized charge carrier $n(t)$ and photon $s(t)$ densities, and rescaling $N(t) = n(t)N_{th}$ and $S(t) = s(t)S_0$, where $S_0 = \Gamma(\tau_p/\tau_n)N_{th}$ and $N_{th} = N_0 + (\Gamma g_0 \tau_p)^{-1}$ is the threshold carrier density; time is normalized to the characteristic LC resonant tank frequency, $\omega_0 = (\sqrt{LC})^{-1}$, hence $\tau = \omega_0 t$. Finally, redefining τ as t, and introducing into the system the delayed feedback $\eta s(t-\tau_d)$, where η is the feedback strength and τ_d is the time-delay with respect to the dimensionless time t, the Liénard oscillator-laser diode dynamical system is transformed into the following dimensionless coupled DDEs:

$$\dot{x}(t) = \frac{1}{\mu}\left[y(t) - f(x) - \chi\xi(t) - \eta s(t-\tau_d)\right] \tag{8}$$

$$\dot{y}(t) = \mu\left[v_0 - \gamma\, y(t) - x(t)\right] \tag{9}$$

$$\dot{n}(t) = \frac{1}{\tau_n'}\left[\frac{i_m(t)}{i_{th}} - n(t) - \frac{n(t)-\delta}{1-\delta}\{1-\epsilon s(t)\}s(t)\right] \tag{10}$$

$$\dot{s}(t) = \frac{1}{\tau_p'}\left[\frac{n(t)-\delta}{1-\delta}\{1-\epsilon s(t)\}s(t) - s(t) + \beta n(t)\right]. \tag{11}$$

Equations (8)–(11) represent the system of equations of the RTD-PD-LD with delayed feedback control through the variable $s(t-\tau_d)$. The feedback strength η parameter depends on RTD-PD detection characteristics, Eq. (3), and the fraction of the laser optical output power P_f reinjected into the delayed feedback loop, Eq. (7). Equations (8), (9) represent the Liénard oscillator where the function $f(x)$ comes from the normalization of $F(V)$, and $\mu = V_0/I_0\sqrt{C/L}$ is a dimensionless parameter. Equations (10), (11) are the dimensionless rate equations describing LD normalized photon $s(t)$ and injected carrier $n(t)$ densities. The charge carrier in the laser Eqs. (10), (11) is normalized to threshold as in [28]; $i_m(t)$ accounts for the bias current and the fraction of the output current oscillations produced by RTD-PD electrical model, Eqs. (8), (9), that modulate the LD, and i_{th} is the dimensionless laser diode threshold current. The parameters τ_n' and τ_p' come from the time rescaling. Table II presents the dimensionless parameters used in the numerical simulations.

In real systems, the unavoidable noise sources affect the dynamics by introducing amplitude and phase fluctuations even in the most stable periodic signals. In our case, several sources or random processes are at play, like e.g. thermal and shot noises. We model their overall effect as an effective delta-correlated Gaussian white noise of zero mean $\chi\xi(t)$ [29], Eq. (8), where the parameter χ is the dimensionless variance of the distribution and denotes the noise strength.

For purposes of numerical simulation, Eqs. (8)–(11) were integrated with a standard constant step size Runge-Kutta method of fourth order [30]. As discussed previously, since long run simulations and large amount of memory storage are required, we interfaced a C++ time integrator with MATLAB & Octave [31] via the mex interface [32]. This allows for high performances, efficient scripting capabilities as well as easy cluster deployment, three characteristics that are useful for extended parametric studies. The presence of a delayed contribution in Eq. (8) demand a special care. Indeed, to advance the solution with a step h from $t_n = nh$ to $t_{n+1} = (n+1)h$, the Runge-Kutta algorithm requires evaluating the values of $s(t-\tau_d)$ at intermediate points $t_{mid} = (n+1/2)h$. However, $s(t_{mid} - \tau_d)$ is not known and must be interpolated from past values, e.g., $s(t_{n-1} - \tau_d)$, $s(t_n - \tau_d)$, $s(t_{n+1} - \tau_d)$, etc., with an order consistent with the algorithm of integration. Therefore, in addition of the past values of $s(t)$ we also kept the time derivative $\dot{s}(t)$, that is, a quantity readily available upon time integration which allows building a third order Hermite polynomial between $t_n - \tau_d$ and $t_{n+1} - \tau_d$. By evaluating this interpolant of the delayed term at $t_{mid} - \tau_d$, we ensure an overall fourth order accuracy. The stochastic noise contribution $\chi\xi(t)$ in Eq. (8) is added after the deterministic step by simply using the Euler method [29]. Figure 6 presents a block diagram showing the corresponding mathematical representation of the OEO model.

In what follows the noise contribution in RTD-based OEO dynamical systems is discussed and the typical physical values of the noise intensities are derived.

TABLE II
PARAMETERS USED IN THE RTD-OEO SIMULATION

Symbol	Parameter	Value
μ	$V_0/I_0\sqrt{C/L}$	3.238×10^{-2}
γ	$R(I_0/V_0)$	7.8
τ_n'	Dimensionless carrier lifetime	0.30578
τ_p'	Dimensionless photon lifetime	0.01395
δ	N_0/N_{th}	0.613
ϵ	$\epsilon_n S_0$ (dimensionless laser gain saturation)	1.72×10^{-3}
β	Spontaneous emission	4×10^{-4}

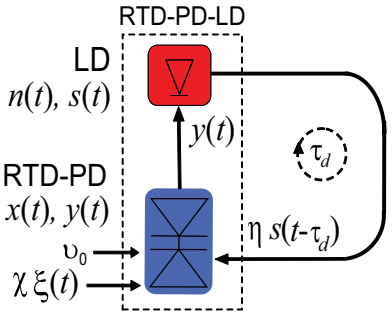

Fig. 6. Block diagram of the delayed feedback Liénard laser diode dimensionless system.

D. Noise in RTD-PD OEO Systems

The fundamental noise sources in the RTD-PD OEO system consist of thermal noise, shot noise, and laser relative intensity noise (RIN), which for the purpose of analysis can be viewed as all originating from the photo-detector, since the photo-detector is monolithically integrated with the RTD structure. Therefore, we are mainly interested in the thermal and shot noise sources of the RTD-PD. In an RTD-PD device, thermal noise or Johnson noise consists of thermal induced random fluctuations in the charge carriers of the materials with finite resistivity. These fluctuations are characterized by a Gaussian random process and they can be modeled as an equivalent current noise source in parallel with a noise-free resistor. Electronic shot noise is associated with the passage of carriers across a potential barrier such as those encountered in semiconductor $p-n$ junctions of diodes and transistors. The statistics that describe charge motion determine the noise characteristics. When the number of events that occur per unit time observation is large then the Poisson distribution can be replaced by a distribution of a zero mean Gaussian process with a white power spectral density.

The RTD-PD's thermal noise can be estimated from Nyquist generalized formula [33], where the power spectral density is given by:

$$S_T = 4\kappa_B T G \tag{12}$$

with G being the differential conductance of the RTD-PD. For typical RTDs with $G = 0.2$ S at $T = 300$ K we obtain $S_T = 0.33 \times 10^{-20}$ A^2/Hz. The power spectral density of RTD-PD electronic shot noise is given by:

$$S_I = 2e\gamma' I \tag{13}$$

where I is the average current, and γ' is the shot noise factor. In double barrier structures a phenomenon called shot noise suppression has been reported due to the reduction of γ' below 0.5 [34], in the I-V positive differential resistance region, prior to the NDR, see Fig. 4. When the device is DC biased in the NDR, enhanced shot noise is expected with respect of the full shot noise [35]. Here, for simplicity of the model, we are assuming $\gamma' = 1$. Therefore, for a DC current of 25 mA (RTD-PD biased close to the valley region, Fig. 4), we obtain $S_I = 0.8 \times 10^{-20}$ A^2/Hz. These values compare with the RTD current noise caused by shot noise reported in [33] for InGaAlAs structures similar with the ones discussed here.

It is possible to relate the dimensionless noise intensity χ with the physical value of the noise found in experimental RTD-OEO systems considering the thermal and shot noises discussed previously in Eqs. (12) and (13). The parameter χ defines the noise strength and $\xi(t)$ defines the Gaussian distribution added in Eq. (8) after the deterministic step. Therefore, if we want to relate χ to the physical noise intensity values we must pay attention to the time scaling and simulation time step. Since the model of Eqs. (8)–(11) is dimensionless, the time variable t is dimensionless too, and reflects the physical time $\tilde{t}$ in units of $\sqrt{LC} \cong 100$ ps (assuming physical circuit parameters L and C presented in Table I). Furthermore, we use the dimensionless stochastic force χ, with I_0 as the scale parameter of the physical dimension of current (here $I_0 = 1$ A). Therefore the dimensionless noise is given by:

$$\chi = (\sigma_T + \sigma_I)/I_0 = \left(\sqrt{4\kappa_B T G/\tau_a} + \sqrt{2q\gamma' I/\tau_a}\right) \Big/ I_0 \tag{14}$$

where σ_T and σ_I, are the thermal and shot noises in units of current, respectively, and $1/\tau_a$ is the bandwidth to be examined (equal to sampling frequency). For a typical time step used in the simulations of $h = 0.01$ (corresponding to a time scale of 1 ps which is of the order of magnitude of typical Johnson noise correlation at room temperature), and considering the values used to calculate the power spectral densities presented previously in Eqs. (12) and (13), we obtain a typical χ level of around 1.5×10^{-4}.

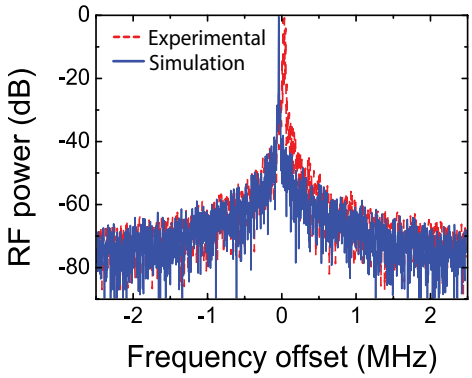

Fig. 7. Experimental RF power spectrum of RTD-PD-LD free-running electrical output (dashed line), and simulated (continuous line) power spectrum of free-running fundamental oscillation of $x(t)$ output with noise contribution $\chi = 5 \times 10^{-4}$. In both plots, the span was 5 MHz and the central frequency was 1.12207 GHz.

Figure 7 shows a typical experimental RF power spectrum of a free-running RTD-PD-LD electrical output at around 1.12207 GHz, and the simulated power spectrum of the voltage $x(t)$ at approximately the same oscillation frequency with noise contribution for parameters shown in Table II. The introduction of noise with amplitude $\chi = 5 \times 10^{-4}$ into the system produces a broader peak in the Fourier domain. Also observed is a reduction of the signal-to-noise ratio at the free-running oscillation frequency. This value of noise amplitude fits relatively well with the experimental data. In what follows, we consider the noise value constant and for simplicity of analysis we define the new parameter $\theta = \eta/\chi$ that stands for the feedback strength to noise ratio of the Liénard OEO system.

IV. Single Loop Results and Discussion

When the time delayed feedback is included diverse dynamical effects are observed namely close-to-carrier noise reduction and the appearance of side modes due to the delay contribution.

We have modeled these behaviors using three round trip times $\tau_d \cong 2.35$ μs, $\tau_d \cong 4.25$ μs, and $\tau_d \cong 6.09$ μs, which correspond to the fiber lengths of 0.4 km, 0.8 km, and 1.2 km, respectively, utilized in the experiments. The

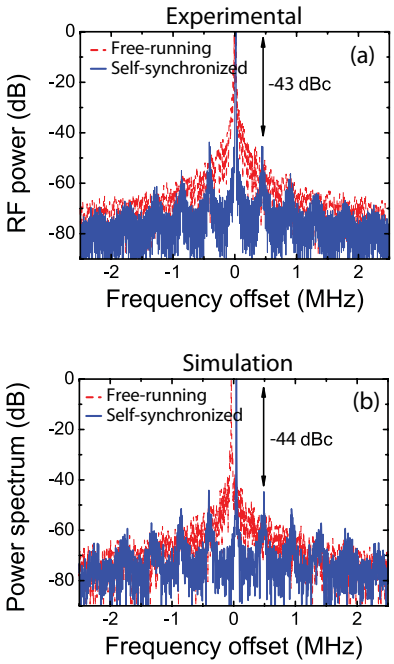

Fig. 8. (a) Experimental RF power spectra of free-running oscillation and self-synchronized electrical output at $P \sim 6$ dBm and 0.4-km fiber length. (b) Simulated power spectra of free-running fundamental oscillation and self-synchronized $x(t)$ outputs with time delay of $\tau_d = 2.35$ μs and feedback strength to noise ratio of $\theta = 2.0$. In both plots, the span was 5 MHz and the central frequency was 1.12207 GHz.

round trip times were obtained from the free-spectral range (FSR) of experimental results, which in our case depends on the electrical time delay τ_e, introduced by the electrical components, and on the optical time delay τ_o, due to optical fiber length:

$$FSR = \frac{1}{\tau_e + \tau_o} \tag{15}$$

For long feedback routes (optical fiber lengths above 1 km) the optical time delay is much larger than the electrical time delay, and $\tau_d \cong \tau_o = n_F L_f / c$, with n_F being the optical fiber effective refractive index, L_f the fiber length, and c the velocity of light.

Equations (8)–(11) were integrated with a time step of $h = 0.01$, which corresponds to $dt = 1$ ps, over l round trips in the external fiber loop. At each round trip the signal was propagated in the OEO and computed according to the Runge-Kutta algorithm described previously. In order to avoid very long time simulations and large memory requirements, we have chosen round trip times up to $\tau_d \cong 6.09$ μs and a time sampling of 10, i.e., 1 point every 10 was sampled.

Figure 8 presents the experimental (a) and simulated (b) power spectra around the fundamental free-running oscillation with and without delayed feedback. Figure 8(a) presents the experimental results of self-synchronized electrical output using an in-fiber optical re-injected power P of ~ 6 dBm and 0.4 km fiber length. The results show phase noise and linewidth reductions at offsets below 250 kHz of the carrier frequency, and side-modes separated by about 425 kHz with a single mode suppression ratio (SMSR) of -43 dBc. Note that the linewidth of the self-synchronized output could not be resolved by the 3 kHz resolution limit set by the instrument.

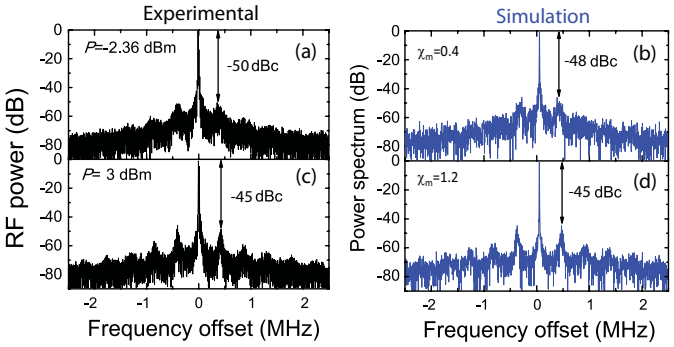

Fig. 9. Experimental RF power spectra of self-synchronized electrical output. (a) $P \sim -2.36$ dBm and (c) $P \sim 3$ dBm for 0.4-km fiber length. Simulated power spectra of self-synchronized $x(t)$ outputs with time delay $\tau_d = 2.35$ μs and feedback strength to noise ratio. (b) $\theta = 0.4$. (d) $\theta = 1.2$. In all plots, the span was 5 MHz and the central frequency was 1.12207 GHz.

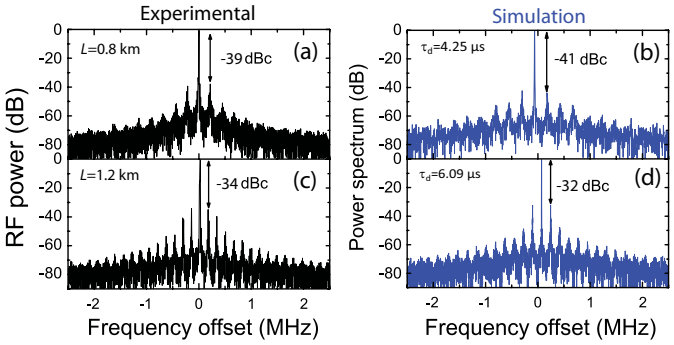

Fig. 10. Experimental RF power spectra of self-synchronized electrical output at $P \sim 3$ dBm for (a) 0.8-km and (c) 1.2-km fiber lengths. Simulated power spectra of self-synchronized $x(t)$ outputs with time delay. (b) $\tau_d = 4.25$ μs and (d) $\tau_d = 6.09$ μs, and fixed feedback strength to noise ratio of $\theta = 1.2$. In all plots, the span was 5 MHz and the central frequency was 1.12207 GHz.

Figure 8(b) shows the corresponding simulation for a time delay of $\tau_d = 2.35$ μs, and a feedback strength to noise ratio of $\theta = 2.0$ (corresponding to a feedback strength $\eta = 1 \times 10^{-3}$, for an injected optical power of 6 dBm). As observed experimentally, the introduction of time delayed feedback variable in the Liénard OEO model narrows the linewidth of the fundamental oscillation frequency and generates frequency side peaks due to the time-delay τ_d, which corresponds to the FSR of the RTD-OEO system. The SMSR of -44 dBc compares with the experimental result shown in Fig. 8(a).

Figure 9 shows the dynamics of the RTD-OEO as a function of the optical power level for a fixed delay, $\tau_d = 2.35$ μs. The minimum experimental optical power threshold necessary to self-synchronize the RTD-OEO and observe the presence of the side-modes close to the noise floor was around -2.36 dBm, Fig. 9(a), and compares with the simulated results at a feedback strength to noise ratio of $\theta = 0.4$, Fig. 9(b). As the optical power increases, the reduction of noise close to the carrier frequency also improves. However, the presence of the side modes with SMSR around -45 dBc deteriorates the spectra at offsets around the FSR, as demonstrated experimentally and numerically in Figs. 9(c) and (d), respectively.

In Fig. 10 we investigate the influence of increasing the time delay in the dynamics of the RTD-OEO at a fixed

feedback strength to noise ratio, $\theta = 1.2$. When $\tau_d = 4.25\ \mu s$ the side modes are present at levels around -39 dBC and -41 dBc in the experimental and simulated results, Figs. 10(a) and (b), respectively. The influence of the delay is more pronounced in Figs. 10(c) and (d) for $\tau_d = 6.09\ \mu s$, showing several side modes with a SMSR above -35 dBc. In both the experimental and simulation, the mode spacing decreased from about 236 kHz to 162 kHz when the delay line was increased from 0.8 km to 1.2 km. The results provide evidence that there is a compromise between the delay and the oscillator stability because increasing the time delay produces higher power side peaks close to the carrier. To overcome this limitation configurations using multiple delayed-feedbacks paths were implemented to suppress the side modes [13]–[15], as demonstrated in the next section.

The model dynamics investigated here describes the dynamics observed experimentally where the characteristics of the OEO are controlled using a delay line. The large number of side-bands spaced by FSR (inversely proportional to the time delay) is an indication that more complex dynamics may occur, strongly depended of the feedback level and the length of the external cavity. In the results presented here, considering the moderate levels of feedback employed, $\eta << \Delta I/I_0$, where ΔI is the peak-to-valley current ratio, only stable self-synchronized oscillations were observed.

V. Dual-Loop RTD-OEO

As verified in the previous section, a disadvantage of using a single fiber loop is the production of side mode oscillations. These modes - highly undesirable for certain applications - are caused by the propagation of waves multiple times around the OEO loop. There are two effective solutions for the removal or suppression of side modes. One scheme involves using multiple feedback loops of fiber, which essentially functions as a set of narrow band filters. Other techniques employ high-Q optical cavities to filter out the unwanted modes [36].

Yao and Maleki demonstrated a dual loop OEO configuration where the optical power was split by an optical decoupler with both portion of the optical signal being subsequently detected by two photo-detectors [13]. The two converted RF signals were coupled by an RF coupler and then fed to the E-O modulator after amplification. In each loop, the process was equivalent to a single-loop OEO. In this configuration, the method uses the natural structure of the OEO cavity to obtain filtering through an additional fiber loop or loops having shorter lengths, in parallel with the long fiber loop. Although this design gave the expected result, two high-speed photodetectors were needed.

Here, we investigate substantial improvements in the level of the side modes of oscillations using a carrier suppression scheme in a dual loop RTD-OEO configuration with a single RTD-PD device. As illustrated in Fig. 11, a portion of the laser optical output is split into two parts each propagating through fibers having different lengths and then combined in a single fiber to be coupled to the single RTD-PD. That is, the RF signals are coupled in the optical domain without adding extra active electrical or optoelectronic devices. Due to the interference between the two combined optical signals the dual loop RTD-OEO presents strong mode selectivity with low power side modes, although it may suffer of problems related with coupling in the optical domain, namely interference and beating.

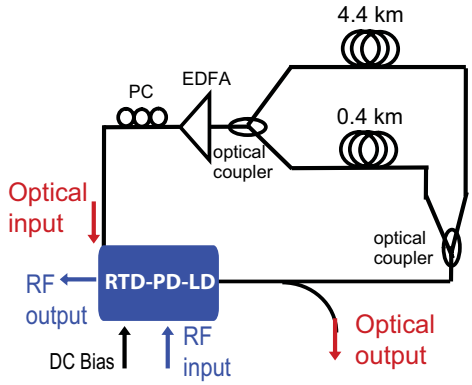

Fig. 11. Schematic diagram of the dual-loop self-synchronized RTD-OEO setup.

In what follows, we present the experimental and simulated results of the dual-loop RTD-OEO configuration, and compare our RTD-OEO with state of the art dual loop OEOs.

A. Results

The dual-loop RTD-OEO using a 4.4 km and a 0.4 km fiber loop lengths, Fig. 11, was investigated experimentally measuring the phase noise and level of side modes characteristics. The longer fiber leads to high spectral purity and low phase noise at low offsets. The short fiber is able to suppress the side modes close to the carrier. Breaking either path, there is a complete single-loop OEO, which is able to freely run, as demonstrated in the previous section. With the long path broken (4.4 km fiber loop), the mode spacing is 425 kHz and the measured side mode suppression ratio was -53 dBc at $P \sim 6$ dBm [see Fig. 12(a)]. With the short path broken (0.4 km fiber loop), the mode spacing is 45 kHz and the measured side mode suppression ratio was around -20 dBc [see Fig. 12(b)]. In the case of the dual-loop configuration, the side mode suppression ratio was improved up to -60 dBc [see Fig. 12(c)]. Compared with the single-loop results, the side modes can be effectively suppressed by 20–40 dB, depending of the optical power input launched into the RTD-PD.

The single side band (SSB) phase noises of the single [Fig. 13(a)] and dual loop [Fig. 13(b)] configurations were measured. The phase noise at 10 kHz away from the carrier of the dual loop RTD-OEO was -99.28 dBc/Hz for 6 dBm in-fiber re-injected optical power, and -102.88 dBc/Hz for 9 dBm optical power [Fig. 13(b)], which compares with the single loop at 4.4 km, showing -101.67 dBc/Hz at 10 kHz away from the carrier [Fig. 13(a)]. Therefore, besides maintaining the quality of the phase noise below -100 dBc/Hz at low offset, successfully suppression of the side modes was achieved in the spectral region above 45 kHz frequency offset of the carrier frequency which confirms the efficient side mode suppression function of the dual loop configuration.

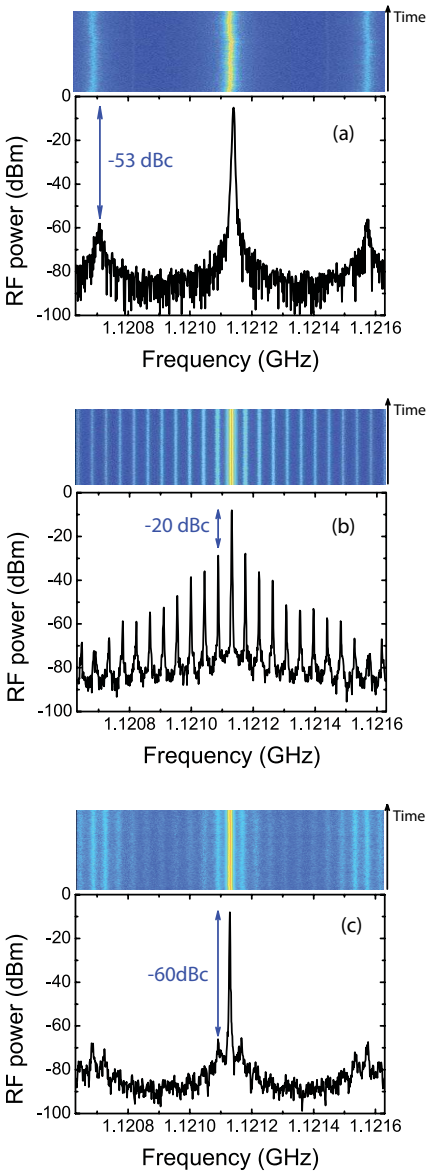

Fig. 12. RF power spectra output showing the SMSR. (a) 0.4-km single loop. (b) 4.4-km single loop. (c) Dual-loop configuration. The frequency span and resolution bandwidth settings were 1 MHz and 3 kHz, respectively. The top part of each figure shows a spectrogram that represents the evolution of spectral density recorded over 1 min (temporal time in the vertical axis).

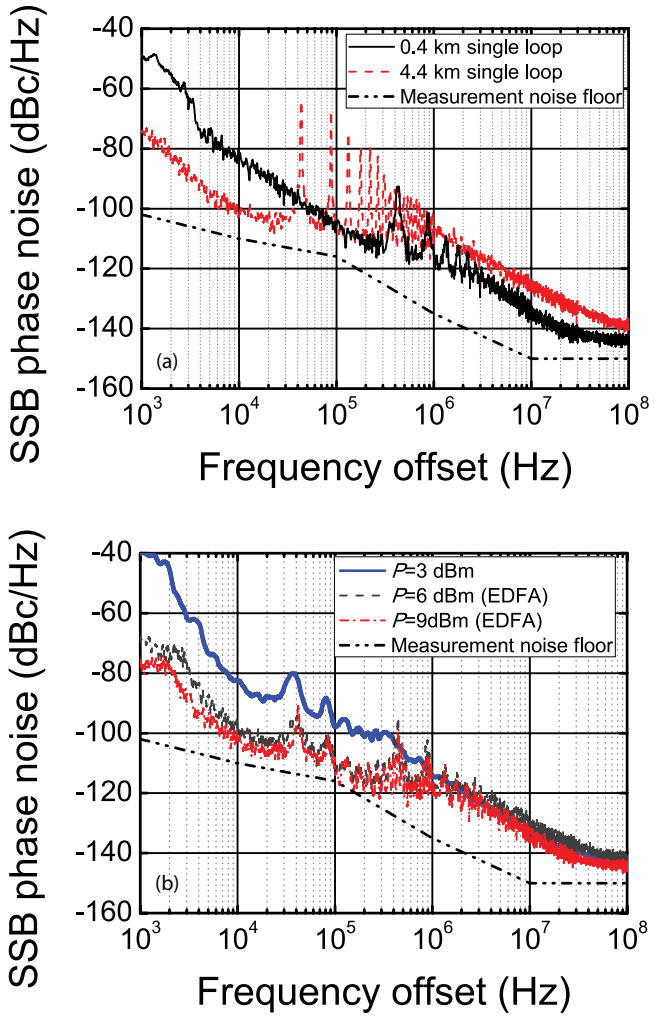

Fig. 13. SSB phase noise plots. (a) 0.4-km and 4.4-km single-loop paths at $P \sim 6$ dBm optical power. (b) Dual-loop configuration with and without EDFA.

The measurements also showed that little close-to-carrier noise is introduced by the dual-loop configuration resulting sometimes in poor noise levels at lower carrier offsets when compared with the single 4.4 km long path; these effects can be reduced or eliminated using polarization maintaining fibers.

Figure 13(b) also shows results of a similar dual-loop setup without using optical amplification at $P = 3$ dBm, which demonstrate a dual-loop RTD-OEO not requiring either electrical or optical amplification. The erbium doped fiber amplifier (EDFA) was used in the dual loop experiments to compensate the losses of coupling the light in more than one fiber, and due to the experimental difficulties of coupling and decoupling light in free-space conditions, since the waveguide RTD-PD was not optimized for this application.

Finally, we demonstrate that the dual loop Liénard OEO numerical model also describes the observed experimental results. We use Eqs. (8)–(11), with a modification in Eq. (8) to include two time delay contributions from the dual-loop configuration. Therefore, we change the single feedback from $\eta s(t - \tau_d)$ to the dual feedback $\eta_1 s(t - \tau_1) + \eta_2 s(t - \tau_2)$ where $\tau_1 < \tau_2$. Such a simple addition of the two photocurrents sources can be performed since after such a long propagation time the two signals are not coherent anymore with respect to each other. As such their interference average out. In addition, the fiber being not polarization preserving means the two re-injected signals may also have partially orthogonal polarizations.

In the numerical simulations we have chosen the round trip times $\tau_1 \cong 2.35$ μs and $\tau_2 \cong 22.2$ μs, which correspond to the fiber lengths of 0.4 km and 4.4 km, respectively, used in the dual loop experiments. In Fig. 14 we present a comparison between experimental data and simulated power spectra. Figures 14(a) and (b) show the experimental and simulated multimode oscillation, respectively, of a single-loop RTD-OEO (in which the shorter loop is disconnected).

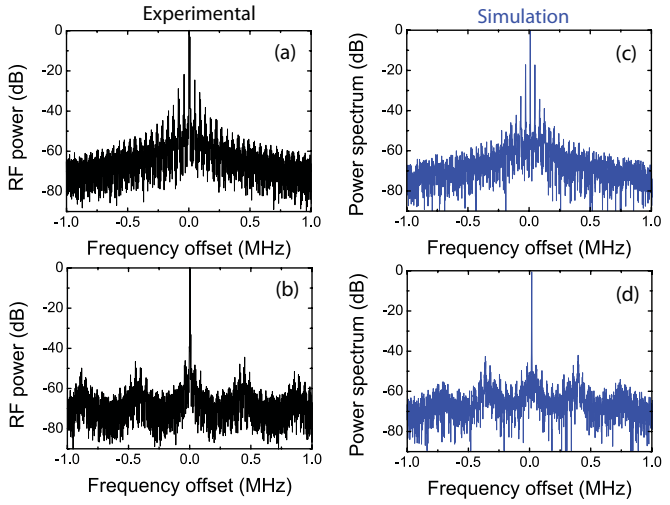

Fig. 14. (a) Experimental RF power spectra of self-synchronized electrical output at $P \sim 0$ dBm and 4.4-km fiber length and (b) dual-loop configuration. Simulated power spectra of self-synchronized $x(t)$ outputs. (c) Single delay at $\theta = 0.3$ and (d) dual delay at feedback strength to noise ratios $\theta_1 = 1.0$ (shorter delay), and $\theta_2 = 0.3$ (longer delay). In all plots, the span was 2 MHz and the central frequency was 1.12219 GHz.

TABLE III
COMPARISON OF RECENTLY REPORTED DUAL LOOP OEO CONFIGURATIONS USING OPTICAL FIBER DELAY LINES

Parameter	RTD	Dual OEO (Yao *et al.*) [13]	Laser Optical Injection [14]	Amplifier-Less OEO [15]
Frequency (GHz)	1.12	10	15	10
Fiber-loops 1/2 length (km)	4.4/0.4	2/0.004	10/1.7	2.3/1.4
Phase noise @ 10 kHz (dBc/Hz)	−102.88	−140	−104	−120
SMSR (dBc)	60	>60	>70	>70
RF amplification	No	Yes	Yes	No
External modulator	No	Yes	Yes	Yes
RF filter	No	Yes	Yes	Yes
EDFA	Yes	No	Yes	Yes
Lasers[a]	1	1	2	1
Photo-detectors[a]	1	2	1	2

[a] Number of components.

Figures 14(c) and (d) present the single-mode oscillation of a dual-loop RTD-OEO in which both loops are closed. It is evident that the presence of the shorter loop effectively suppresses the side modes of the longer loop and only leaves the fundamental oscillation signal. In both experimental and simulated results we can also observe the presence of additional side modes due to the shorter fiber with a spacing of about 425 kHz with an interference pattern that results of the combination of the two delayed-feedback signals. In Fig. 14(d) the SMSR is −48 dBc which is in a good agreement with the experimental value of −51 dBc presented in Fig. 14(c). The results clearly demonstrate the model presented here can be extremely useful for design purposes to select the appropriate cavity characteristics to achieve efficient suppression of side modes.

B. Comparison With State of the Art OEOs

A considerable number of single and dual loop OEO alternatives has been proposed in the last decade followed by the first demonstration of the dual-loop OEO by Yao et al. [13]. Table III compares the performance of the RTD-OEO and various state of the art dual loop OEOs that use optical fiber delay lines. Although in terms of phase noise and oscillation frequency the RTD-OEO presents a lower figure of merit, the dual loop OEO implementation reported here uses only a single RTD-PD which reduces considerably the number of components usually required in dual-loop OEO configurations with the advantage of simplifying the RF and optoelectronic part of the loop. Other configurations have been also reported in order to reduce the number of components in the OEO, namely the amplifier-less OEO [15], Table III. However, in many cases there is a limit for the optical gain in the fiber when high power lasers are used to provide the RF gain due to the increasing of the associated RIN noise. In addition, stimulated Brillouin scattering also limits the loop lengths to a few km using laser power at tens of mW, which limits the maximum Q factor of these configurations.

We also found RTD-OEO's phase noise levels are below the performance of the best available quartz oscillators [37], and dielectric resonator oscillators (DROs) [38] that show phase noise levels as low as −159 dBc/Hz at 10 kHz offset from the carrier frequency operating ∼1 GHz. However, unlike the resonator technology where the dielectric losses at higher microwave frequencies limits the attainment of unloaded quality factors higher than 10^5, the RTD-OEO approach reported here using optical techniques is potentially suitable for generating microwave signals >10 GHz (only limited by the modulation bandwidth of the laser diode) in both optical and electrical domains, and with extremely low phase noise taking advantage of the long low-loss optical delay lines to maximize the quality factor. Moreover, the fiber loop is not an essential part of the RTD-OEO since the fiber loop in future work can be replaced by very high-Q micro optical resonators (e.g. whispering gallery modes) in single chip integration configurations where miniaturization is essential, as reported in [36].

Considering there is still scope for optimization in many aspects of the dual-loop RTD-OEO configuration including RTD-PD efficiency, and optical fiber temperature and vibration control, the OEO topologies using self-injection locking of RTD oscillators can be interesting alternatives for novel low cost OEOs, simple and of miniature size configurations that could greatly increase the practicality of OEOs in a wider range of microwave and photonics applications.

VI. CONCLUSION

We have successfully demonstrated a simplified optoelectronic oscillator in both single and dual loop configurations operating in the gigahertz range using resonant tunneling diode photo-detectors and laser diodes without the need for extra

electrical amplifiers, photo-detectors or external modulators. We achieved low phase noise of −102.88 dBc/Hz at 10 kHz offset of 1.12 GHz center frequency with a side mode suppression ratio of −60 dBc. Further developments of this RTD-based OEO configuration could increase the practicality of OEOs in a wide range of microwave photonics applications.

We have also shown a numerical model based upon delay differential equations to investigate the dynamics of resonant tunneling diode photo-detector optoelectronic oscillators in both single and dual loops. The Liénard-laser diode oscillator model with time delayed feedback and driven by white Gaussian noise provides a good qualitative and semi-quantitative analysis of RTD-OEO circuits; the numerical simulations presented here are in a good agreement with our experimental results predicting the free-spectral range and the side mode suppression main features of RTD-OEOs. The model can be used either to map the RTD-OEO dynamical regimes in order to avoid unstable regions or to take advantage of the rich dynamics which can be used to investigate innovative applications such as generation of electrical and optical frequency combs [2], or even chaotic transitions [5] controlled by the delayed feedback parameter. Extensions of this model are numerous. The Liénard RTD-OEO model can be modified to include additional physical effects of the RTD-PD associated with its optical response [27], and other noise contributions of a typical OEO such as flicker noise from environmentally driven changes in the fibers, which will enable to help users to design OEOs based on RTD-PD devices.

REFERENCES

[1] T. Erneux, *Applied Delayed Differential Equations*. New York: Springer-Verlag, 2009.

[2] X. Y. Yao and L. Maleki, "Optoelectronic oscillator for photonic systems," *IEEE J. Quantum Electron.*, vol. 32, no. 7, pp. 1141–1149, Jul. 1996.

[3] K. Ikeda and K. Matsumoto, "High-dimensional chaotic behavior in systems with time-delayed feedback," *Phys. D*, vol. 29, nos. 1–2, pp. 223–235, 1987.

[4] T. E. Murphy, A. B. Cohen, B. Ravoori, K. R. B. Schmitt, A. V. Setty, F. Sorrentino, C. R. S. Williams, E. Ott, and R. Roy, "Complex dynamics and synchronization of delayed-feedback nonlinear oscillators," *Phil. Trans. Royal Soc. A*, vol. 368, pp. 368–343, Feb. 2010.

[5] K. E. Callan, L. Illing, Z. Gao, D. J. Gauthier, and E. Scholl, "Broadband chaos generated by an optoelectronic oscillator," *Phys. Rev. Lett.*, vol. 104, no. 11, pp. 113901-1–113901-4, 2010.

[6] L. Illing, D. J. Gauthier, and R. Roy, "Controlling optical chaos, spatio-temporal dynamics, and patterns," *Adv. Atomic, Molecular, Opt. Phys.*, vol. 54, pp. 615–697, Mar. 2006.

[7] M. Peil, M. Jacquot, Y. K. Chembo, L. Larger, and T. Erneux, "Routes to chaos and multiple time scale dynamics in broadband bandpass nonlinear delay electro-optic oscillators," *Phys. Rev. E*, vol. 79, no. 2, pp. 045201-1–045201-15, 2009.

[8] S. Tang and J. M. Liu, "Chaotic pulsing and quasi-periodic route to chaos in a semiconductor laser with delayed opto-electronic feedback," *IEEE J. Quantum Electron.*, vol. 37, no. 3, pp. 329–336, Mar. 2001.

[9] R. Lang and K. Kobayashi, "External optical feedback effects on semiconductor injection laser properties," *IEEE J. Quantum Electron.*, vol. 16, no. 3, pp. 347–355, Mar. 1980.

[10] B. Dahmani, L. Hollberg, and R. Drullinger, "Frequency stabilization of semiconductor-lasers by resonant optical feedback," *Opt. Lett.*, vol. 12, no. 11, pp. 876–878, 1987.

[11] J. Mork, B. Tromborg, and J. Mark, "Chaos in semiconductor lasers with optical feedback: Theory and experiment," *IEEE J. Quantum Electron.*, vol. 28, no. 1, pp. 93–108, Jan. 1992.

[12] L. Maleki, D. Eliyahu, and A. B. Matsko, "Optoelectronic oscillator," in *Broadband Optical Modulators: Science, Technology, and Applications*, A. Chen and E. Murphy, Eds. Boca Raton, FL: CRC Press, 2011, pp. 467–488.

[13] X. S. Yao and L. Maleki, "Multiloop optoelectronic oscillator," *IEEE J. Quantum Electron.*, vol. 36, no. 1, pp. 79–84, Jan. 2000.

[14] J.-Y. Kim, J.-H. Jo, W.-Y. Choi, and H.-K. Sung, "Dual-loop dual-modulation optoelectronic oscillators with highly suppressed spurious tones," *IEEE Photon. Technol. Lett.*, vol. 24, no. 8, pp. 7706–708, Apr. 2012.

[15] W. Zhou, O. Okusaga, C. Nelson, D. Howe, and G. Carter, "10 GHz dual loop opto-electronic oscillator without RF-amplifiers," *Proc. SPIE, Optoelectron. Integr. Circuits X*, vol. 6897, p. 68970Z, Feb. 2008.

[16] E. Shumakher, T. Magrisso, S. Kraus, D. C. Elias, A. Gavrilov, S. Cohen, G. Eisenstein, and D. Ritter, "An InP HBT-based oscillator monolithically integrated with a photodiode," *J. Lightw. Technol.*, vol. 26, no. 15, pp. 2679–2683, Aug. 2008.

[17] B. Romeira, K. Seunarine, C. N. Ironside, A. E. Kelly, and J. M. L. Figueiredo, "A self-synchronized optoelectronic oscillator based on an RTD photo-detector and a laser diode," *IEEE Photon. Technol. Lett.*, vol. 23, no. 16, pp. 1148–1150, Aug. 2011.

[18] B. Romeira, J. M. L. Figueiredo, T. J. Slight, L. Wang, E. Wasige, C. N. Ironside, A. E. Kelly, and R. Green, "Nonlinear dynamics of resonant tunneling optoelectronic circuits for wireless/optical interfaces," *IEEE J. Quantum Electron.*, vol. 45, no. 11, pp. 1436–1445, Nov. 2009.

[19] B. Romeira, J. M. L. Figueiredo, C. N. Ironside, A. E. Kelly, and T. J. Slight, "Optical control of a resonant tunneling diode microwave-photonic oscillator," *IEEE Photon. Technol. Lett.*, vol. 22, no. 21, pp. 1610–1612, Nov. 2010.

[20] T. Ramond, L. Hollberg, P. W. Juodawlkis, and S. D. Calawa, "Low-noise optical injection locking of a resonant tunneling diode to a stable optical frequency comb," *Appl. Phys. Lett.*, vol. 90, no. 17, pp. 171124-1–171124-3, Apr. 2007.

[21] A. J. Seeds and K. J. Williams, "Microwave photonics," *J. Lightw. Technol.*, vol. 24, no. 12, pp. 4628–4641, Dec. 2006.

[22] J. M. L. Figueiredo, C. N. Ironside, and C. R. Stanley, "Electric field switching in a resonant tunneling diode electroabsorption modulator," *IEEE J. Quantum Electron.*, vol. 37, no. 12, pp. 1547–1552, Dec. 2001.

[23] M. Feiginov, C. Sydlo, O. Cojocari, and P. Meissner, "Resonant-tunnelling-diode oscillators operating at frequencies above 1.1 THz," *Appl. Phys. Lett.*, vol. 99, no. 23, pp. 233506-1–233506-3, 2011.

[24] J. M. L. Figueiredo, B. Romeira, T. J. Slight, and C. N. Ironside, "Resonant tunnelling optoelectronic circuits," in *Advances in Optical and Photonic Devices*, K. Y. Kim, Ed. Rijeka, Croatia: InTech, 2010.

[25] T. J. Slight, B. Romeira, L. Wang, J. M. L. Figueiredo, E. Wasige, and C. N. Ironside, "A Liénard oscillator resonant tunnelling-laser diode hybrid integrated circuit: Model and experiment," *IEEE J. Quantum Electron.*, vol. 44, no. 12, pp. 1158–1163, Dec. 2008.

[26] J. N. Schulman, H. J. De Los Santos, and D. H. Chow, "Physics-based RTD current-voltage equation," *IEEE Electron Device Lett.*, vol. 17, no. 5, pp. 220–222, May 1996.

[27] I. J. S. Coelho, J. F. Martins-Filho, J. M. L. Figueiredo, and C. N. Ironside, "Modeling of light-sensitive resonant-tunneling-diode devices," *J. Appl. Phys.*, vol. 95, no. 12, pp. 8258–8263, 2004.

[28] Y. H. Kao and H. T. Lin, "Persistent properties of period doubling in directly modulated semiconductor lasers," *Phys. Rev. A*, vol. 48, no. 3, pp. 2292–2298, 1993.

[29] C. W. Gardiner, *Handbook of Stochastic Methods*, H. Haken, Ed. Berlin, Germany: Springer-Verlag, 1985.

[30] W. H. Press, S. A. Teukolsky, W. T. Vetterling, and B. P. Flannery, *The Art of Scientific Computing*. Cambridge, U.K.: Cambridge Univ. Press, 2007.

[31] J. W. Eaton, *GNU Octave Manual*. Surrey, U.K.: Network Theory Publishing, 2002.

[32] *A.2 Mex-Files* (2010) [Online]. Available: http://www.gnu.org/software/octave/doc/interpreter/Mex_002dFiles.html

[33] N. V. Alkeev, V. E. Lyubchenko, C. N. Ironside, J. M. L. Figueiredo, and C. R. Stanley, "Current noise in resonance tunnel diodes based on InGaAlAs heterostructures," *J. Commun. Technol. Electron.*, vol. 47, no. 2, pp. 228–231, 2002.

[34] A. Przadka, K. J. Webb, D. B. Janes, H. C. Liu, and Z. R. Wasilewski, "Microwave measurement of shot noise in resonant tunneling diodes," *Appl. Phys. Lett.*, vol. 71, no. 4, pp. 530–532, 1997.

[35] G. Iannaccone, G. Lombardi, M. Macucci, and B. Pellegrini, "Enhanced shot noise in resonant tunneling: Theory and experiment," *Phys. Rev. Lett.*, vol. 80, no. 5, pp. 1054–1057, 1998.
[36] W. Liang, V. S. Ilchenko, A. A. Savchenkov, A. B. Matsko, D. Seidel, and L. Maleki, "Whispering-gallery-mode-resonator-based ultranarrow linewidth external-cavity semiconductor laser," *Opt. Lett.*, vol. 35, no. 16, pp. 2822–2824, 2010.
[37] T. McClelland, C. Stone, and M. Bloch, "100 MHz crystal oscillator with extremely low phase noise," in *Proc. IEEE Int. Freq. Control Symp. Freq. Time Forum*, vol. 1. Dec. 1999, pp. 331–334.
[38] M. Regis, O. Llopis, B. Van Haaren, R. Plana, A. Gruhle, J. Rayssac, and J. Graffeuil, "Ultralow phase noise C and X band bipolar transistors dielectric resonator oscillators," in *Proc. IEEE Int. Freq. Control Symp.*, vol. 1. May 1998, pp. 507–511.

Bruno Romeira (S'08) received the Diploma degree in physics and chemistry from the University of the Algarve, Faro, Portugal, in 2006. He is currently pursuing the Ph.D. degree with the Center of Electronics Optoelectronics and Telecommunications, University of the Algarve in collaboration with the University of Glasgow, Glasgow, U.K., and the University of Seville, Seville, Spain.

His current research interests include high-speed optoelectronics and nonlinear dynamics of double barrier quantum well resonant tunneling diode devices.

Mr. Romeira was a recipient of the Young Researchers Incentive Programme Award from the Calouste Gulbenkian Foundation, Portugal, in 2009, and the 2011 IEEE Photonics Society Graduate Student Fellowship from the IEEE Photonics Society.

Julien Javaloyes (M'11) was born in Antibes, France. He received the M.Sc. degree in physics from the École Normale Supérieure de Lyon, Lyon, France and the Ph.D. degree in physics from the Institut Non Linéaire de Nice, Université de Nice-Sophia Antipolis, Nice, France, where he studied the recoil induced instabilities and self organization processes occurring in cold atoms.

He worked on delay induced dynamics in coupled semiconductor lasers during a post-doctoral stage in Brussels, and on VCSEL polarization dynamics in Palma de Mallorca. He was a Research Associate with Glasgow University, Glasgow, U.K., where provided for the modeling of the dynamics of monolithic semiconductor diodes. He joined the Physics Department, Universitat de les Illes Balears, Palma, Spain, in 2010, as a Ramón y Cajal Fellow. His current research interests include laser dynamics, atom-light interaction modeling and applied numerical bifurcation analysis.

José M. L. Figueiredo (M'09) received the B.Sc. degree in physics (optics and electronics) and the M.Sc. degree in optoelectronics and lasers from the University of Porto, Porto, Portugal, in 1991 and 1995, respectively.

He was with the Department of Physics, University of Porto, from 1995 to 1999, and with the Department of Electronics and Electrical Engineering, University of Glasgow, Glasgow, U.K., as a Ph.D. student in "co-tutela," working on the optoelectronic properties of resonant tunneling diodes. He is with the Department of Physics, University of the Algarve, Faro, Portugal. His current research interests include electronic and optoelectronic circuits for radio-over-fiber and secure mobile communication systems.

Charles N. Ironside (M'87–SM'05) has been with the School of Engineering, University of Glasgow, Glasgow, U.K., since 1984. He has been engaged in a variety of optoelectronic projects that include ultrafast all-optical switching in semiconductor waveguides, monolithic mode-locked semiconductor lasers, broad-band semiconductor lasers, quantum-cascade lasers, and optoelectronic integrated chip devices, that concentrated on the integration of resonant tunnelling diodes with electroabsorption modulators and semiconductor lasers.

Horacio I. Cantú received the Ph.D. degree in electronics engineering from the University of Manchester Institute of Science and Technology, Manchester, U.K., in 2000.

He is currently a Research Fellow with the Universidade do Algarve, Faro, Portugal. His current research interests include high frequency electronic design, transceiver system integration, and microwave and millimetre wave technologies.

Anthony E. Kelly received the B.Sc., M.Sc., and Ph.D. degrees from the University of Strathclyde, Glasgow, U.K.

He was with the British Telecom Laboratories and Corning. He was also a Co-Founder of Kamelian Ltd., Oxfordshire, U.K., and Amphotonix Ltd., Glasgow. He is currently with the School of Engineering, University of Glasgow. He has authored or co-authored more than 150 journal and conference papers on a range of optoelectronic devices and systems and holds a number of patents. His current research interests include semiconductor optical amplifiers and related devices, visible light communications using GaN devices, and high speed lasers for PON systems.